Nuclear Instruments and Methods in Physics Research A292 (1990) 259–278
North-Holland

MEASUREMENTS OF LONGITUDINAL AND TRANSVERSE PROFILES FOR HADRON SHOWERS IN THE RANGE 10–100 GeV AND COMPARISONS WITH MONTE CARLO SIMULATIONS

The ZEUS Calorimeter Group
F. BARREIRO [1]*, G. CASES [2]**, P. CLOTH [3], K. DIERKS [4], G. DREWS [1], J. ENGELEN [5], D. FILGES [3], M.A. GARCIA [2]+, R. KLANNER [1], U. KÖTZ [1], J. KRÜGER [4], G. LEVMAN [6], J. MARTIN [6], H.-J. MÖHRING [7], F. SELONKE [1], G. STERZENBACH [3], J. STRAVER [5], H. TIECKE [5] and T. TYMIENIECKA [8]

[1] *DESY, Hamburg, FRG*
[2] *Universidad Autónoma de Madrid, Spain*
[3] *Kernforschungszentrum Jülich, FRG*
[4] *II Institute of Experimental Physics, University of Hamburg, FRG*
[5] *NIKHEF-H, Amsterdam, The Netherlands*
[6] *University of Toronto, Canada*
[7] *Sektion Physik, Karl-Marx-Universität, Leipzig, GDR*
[8] *University of Warsaw, Poland*

Received 9 January 1990

Data on the longitudinal and transverse shower profiles initiated by 10, 20, 30, 50, 75 and 100 GeV positive hadron beams are presented. They have been measured with a 6λ deep sampling hadronic calorimeter using 3.2 mm thick depleted uranium plates as absorber and 3.0 mm scintillator layers as active material. The scintillator is read out with wavelength shifter plates coupled to photomultipliers. The data are compared to Monte Carlo calculations, simulating both the development of hadronic cascades as well as detector effects.

1. Introduction

Design studies for the ZEUS experiment [1] have shown [2,3] that hadronic sampling calorimeters, using depleted uranium as absorber and plastic scintillator as active material, compensate if the corresponding thickness ratio is approximately equal to one, as suggested by various Monte Carlo studies [4–6] as well as by early experimental results [7]. The intrinsic and sampling contributions to the energy resolution have been determined as well [8]. The same experimental setup used for these design studies also allows to measure the lateral and longitudinal development of hadron initiated showers. These data are useful for future calorimeter designs and help in the understanding of the performance of hadronic sampling calorimeters as well as in the modelling of hadronic shower Monte Carlos. The aim of this paper is twofold:

- to present data on the doubly differential longitudinal and transverse profiles for hadronic showers in the energy range from 10 to 100 GeV; and
- to make comparisons with current Monte Carlo simulations NEUKA [9] and HERMES [10,11].

2. Experimental details for T60

2.1. Description of the calorimeter

The calorimeter setup consists of four separate modules. Each module consists of 45 depleted uranium (DU) absorber plates, 3.2 mm thick, and 45 scintillator planes (Sc), 3.0 mm thick, see fig. 1a. Between scintillator and absorber plates, 0.2 mm thick stainless steel foils were inserted. The steel foil is meant to reduce the scintillator signal due to the uranium radioactivity while still permitting to use it for calibration purposes. Each module is roughly 1.5 interaction lengths deep. The

* Alexander von Humboldt Fellow, on leave of absence from Universidad Autónoma de Madrid.
** Supported by a Fellowship from Banco Exterior de España.
\+ Partially supported by DGICIT (Spain) and Kernforschungszentrum Karlsruhe (FRG).

0168-9002/90/$03.50

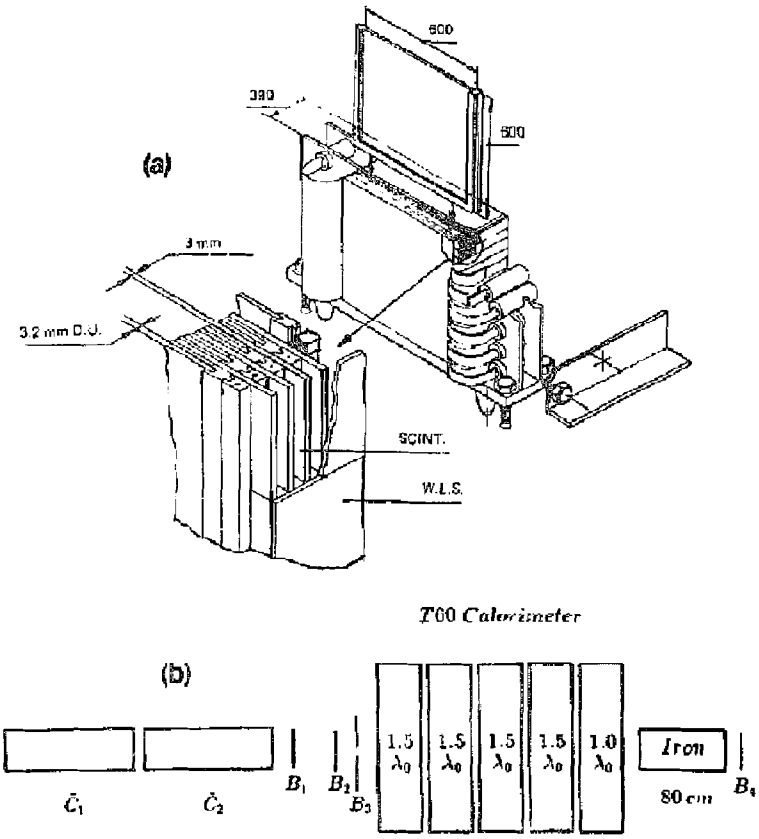

Fig. 1. (a) Schematic layout of a calorimeter module. (b) Schematic layout of the experimental setup.

absorber plates have lateral dimensions of 600×600 mm^2. The scintillator planes are 600 mm high and 625 mm wide. The scintillator planes are 600 mm high and 625 mm wide. The scintillator material used is SCSN-38 [12] and each layer consists of twelve horizontal strips with dimensions of 50×625 mm^2. The scintillator strips, with all sides polished, are wrapped in one layer of white paper and a second layer of aluminized mylar.

A fifth module consisting of 30 layers of 3.2 thick DU plates and 5 mm thick Sc planes, thus with a total depth of 1.1 interaction lengths, was used as a backing calorimeter, to study and correct for longitudinal energy leakage.

The light from each scintillator strip is collected on the left and right sides by a 50 mm wide and 3 mm thick wavelength shifting plate (WLS) made of a PMMA base doped with 120 mg/l K-27 and UV absorbant [13]. Each WLS plate is wrapped with white paper on the side opposite to the scintillator and has all sides polished. In order to make the response of the WLS bar uniform, a graded grey filter was placed between Sc and WLS [14].

The WLS bars, with aluminum end mirrors, are coupled to a Valvo XP-2011 photomultiplier, via a PMMA light guide. The photomultipliers were read out by ADC LRS 2282B which allow gate widths between 40 ns and 10 μs. The gate width used was 150 ns with the gate preceding the rise of the pulses by about 25 ns.

2.2. Experimental setup

The data presented here were taken in runs during July 87 at the CERN XPS X5 test beam area. Fig. 1b schematically shows the setup. Beam particles were defined by two scintillation counters, $10 \times 10 \times 0.2$ cm^3, and a veto counter with a 2 cm diameter hole. Two 10 m long threshold Cherenkov counters were used for beam particle identification. Beams enriched either in hadrons or in electrons could be obtained by different production targets and beam configurations. The calorimeter modules were placed on a movable stand to center the beam onto the individual strips of the calorimeter modules for calibration.

For the calibration two procedures were used:
- uranium radioactivity response,
- muon response.

In the first procedure, the signals from the uranium radioactivity integrated over 10 μs were adjusted to the

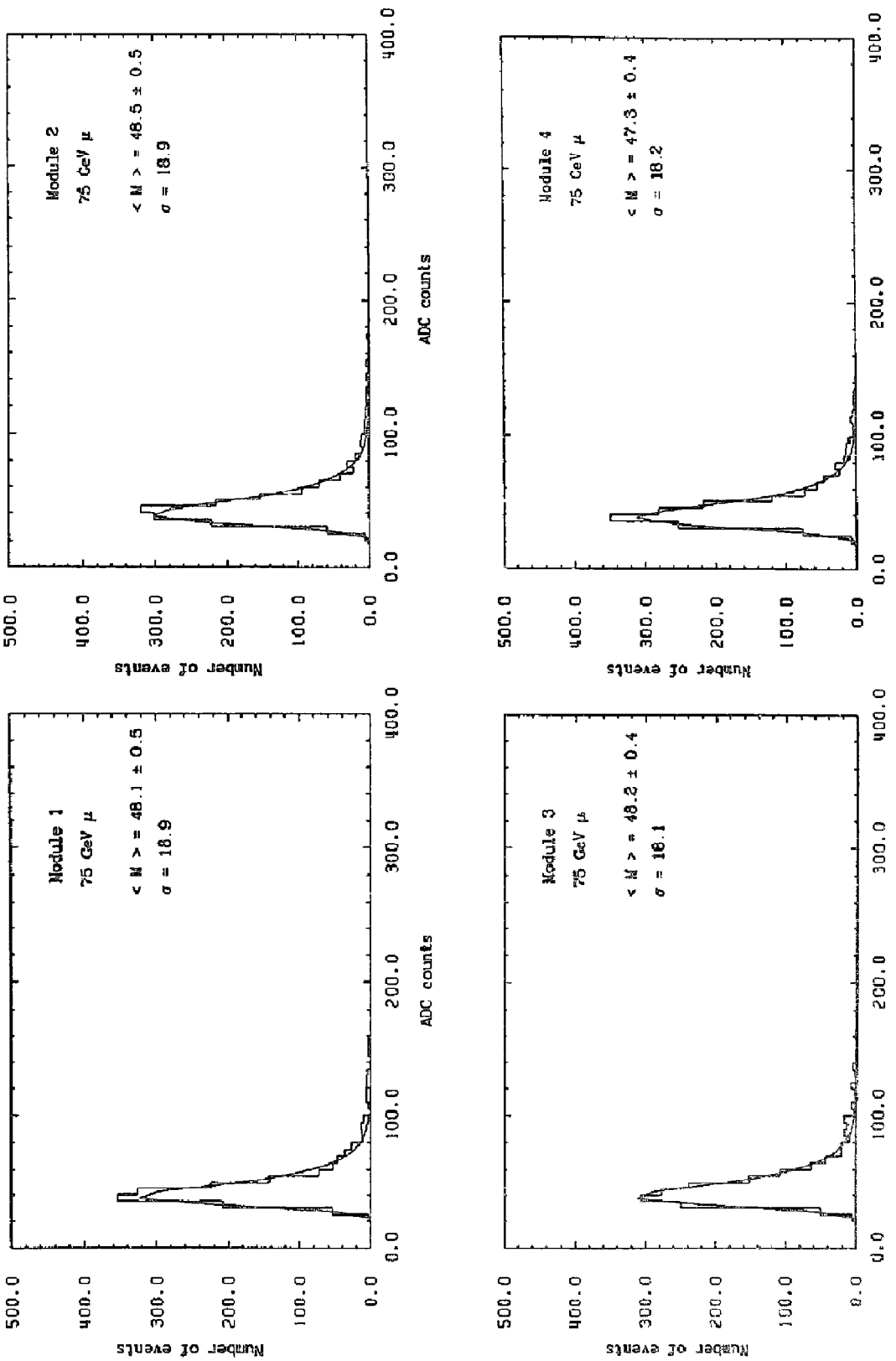

Fig. 2. The signal seen in the sixth strip, for modules 1, 2, 3 and 4 separately when a 75 GeV muon beam impinges upon its center. The solid line represents the results of a fit to a Landau function. The most probable value is determined with a precision less than 1%.

same value. Pedestals for the 10 μs signal were obtained by disconnecting the cables at the input of the ADC.

In the second procedure, we used a 75 GeV muon beam, impinging at the center of every strip. Pedestals were obtained by triggering the ADCs with a 150 ns wide gate signal outside the beam particle burst, then determining the average of the measured pulse height. This obviously includes the uranium radioactivity. The spectra of the photomultipliers at both sides of the strip where the beam was centered, obtained with a 150 ns wide gate generated by the particle burst, were fitted to Landau curves. The calibration constants were then obtained by demanding that all spectra have the same most probable value. The calibration constants thus determined have an accuracy of less than 1% at the time of calibration. For the sake of illustration we show in fig. 2 the signal seen by the sixth strip, in modules 1 to 4 separately, when a 75 GeV muon beam impinges upon its center along with the results of the fits discussed above. Both sets of calibration constants were used to calculate the energy resolution of the calorimeter and the resulting values agreed to better than 1 %.

Since the tails in the shower profiles are very sensitive to pedestals, we have used two additional procedures for their determination, namely

- with electron beams giving rise to profiles fully contained in the first module we were able to check pedestals for modules two to five,
- with muon beams impinging upon the first and the twelfth strip, giving rise to showers fully contained in the strip upon which the muon was incident, we were able to make a complete independent determination of pedestals in the five modules.

The deviations in the measured profiles using these various sets of pedestals were used to infer the systematic error in the data.

Electron, muon and hadron separation was achieved by making use of the two Cherenkov counters as well as of the longitudinal and lateral segmentation of the calorimeter itself. For details we refer to [3]. Unless explicitly otherwise stated and in order to ensure proper longitudinal containment, we used the fifth calorimeter module as a veto calorimeter. A cut at the 2% level of the total energy deposited in the calorimeter was used for that purpose. A total of 3365, 6367, 12528, 9345, 5969 and 2686 hadron events at 10, 20, 30, 50, 75 and 100 GeV respectively, impinging at the center of the seventh strip, remained after this additional cut.

3. Monte Carlo codes

The energy deposited by hadronic showers receives contributions for three basically different mechanisms:

(i) Ionization energy loss of charged hadrons (mainly $\pi^{\pm}$, p, $K^{\pm}$) produced in strong interactions in the calorimeter;

(ii) Energy deposition by electromagnetic showers induced mainly by photons from decaying π^0 and η^0 mesons;

(iii) Nuclear processes, like breakup of highly excited nuclei into strongly ionizing recoiling fragments or subsequent interactions of evaporating neutrons.

Available Monte Carlo codes apply different models and approximations for the description of the various

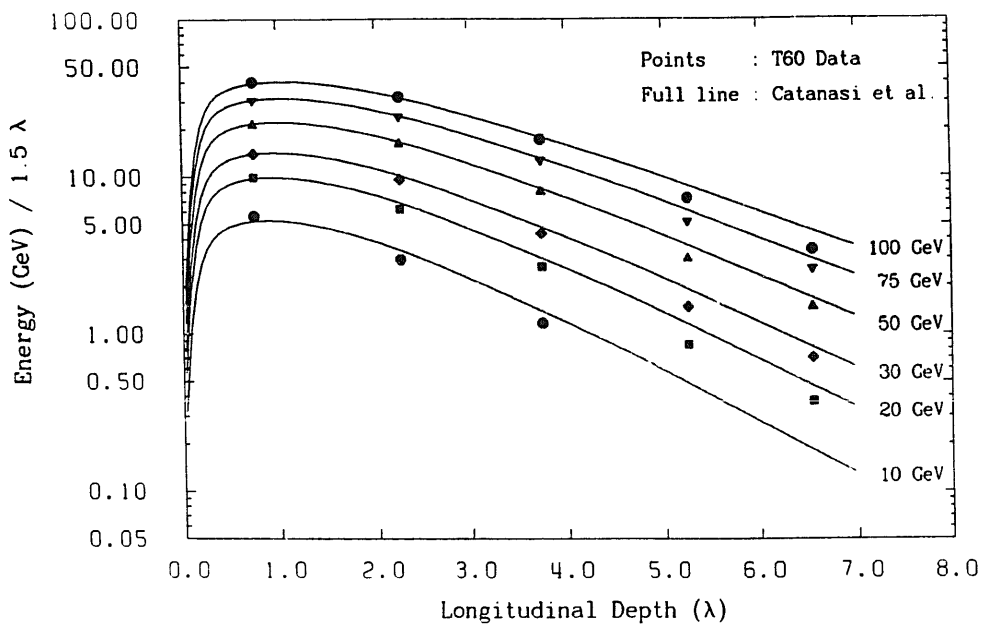

Fig. 3. (a) Longitudinal profiles for hadron showers measured at 10, 20, 30, 50, 75 and 100 GeV (full symbols). The curves represent results of fits performed to describe the WA78 data [26].

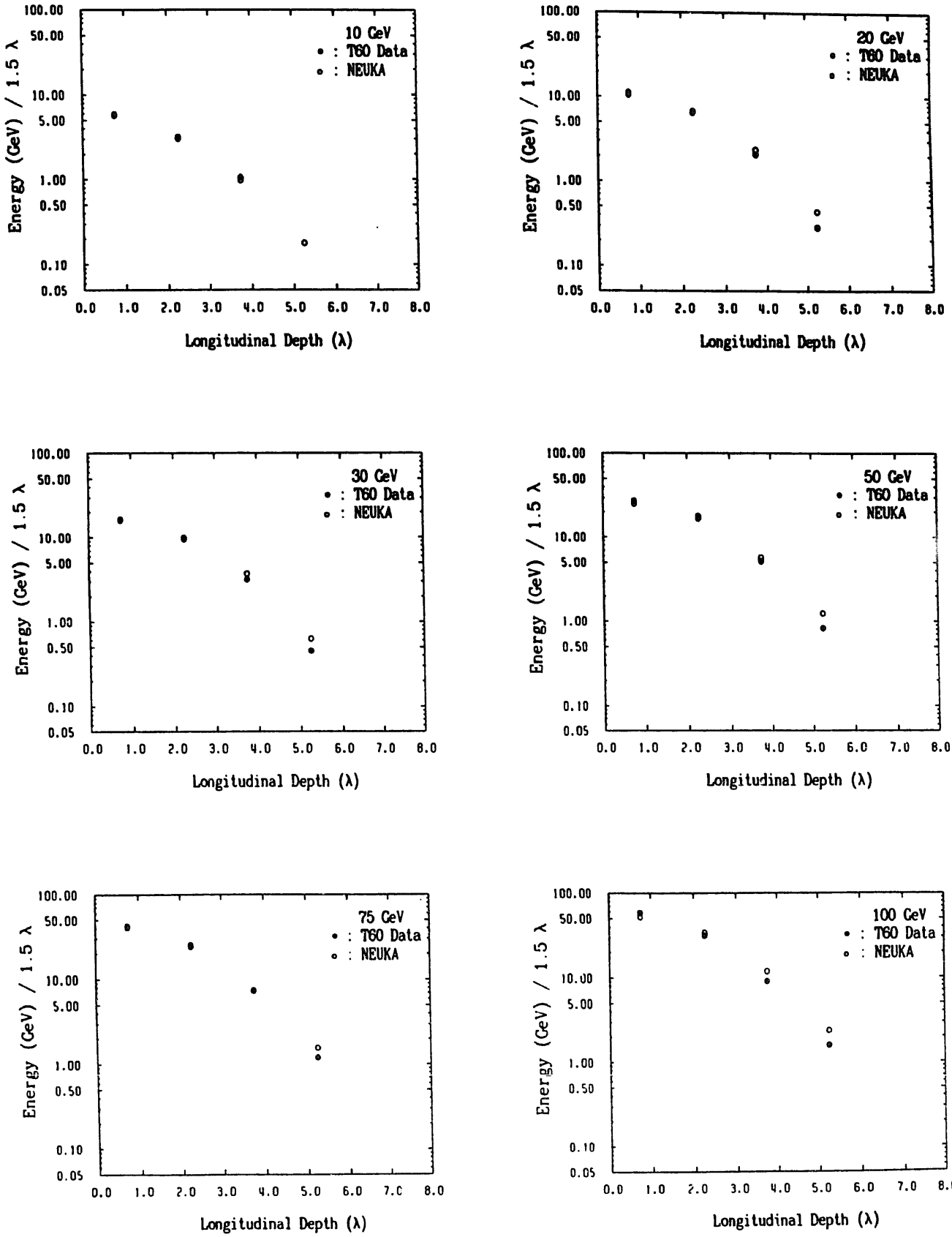

Fig. 3. (b) Longitudinal profiles for fully contained hadron showers measured at 10, 20, 30, 50, 75 and 100 GeV (full symbols) together with expectations in NEUKA (open symbols).

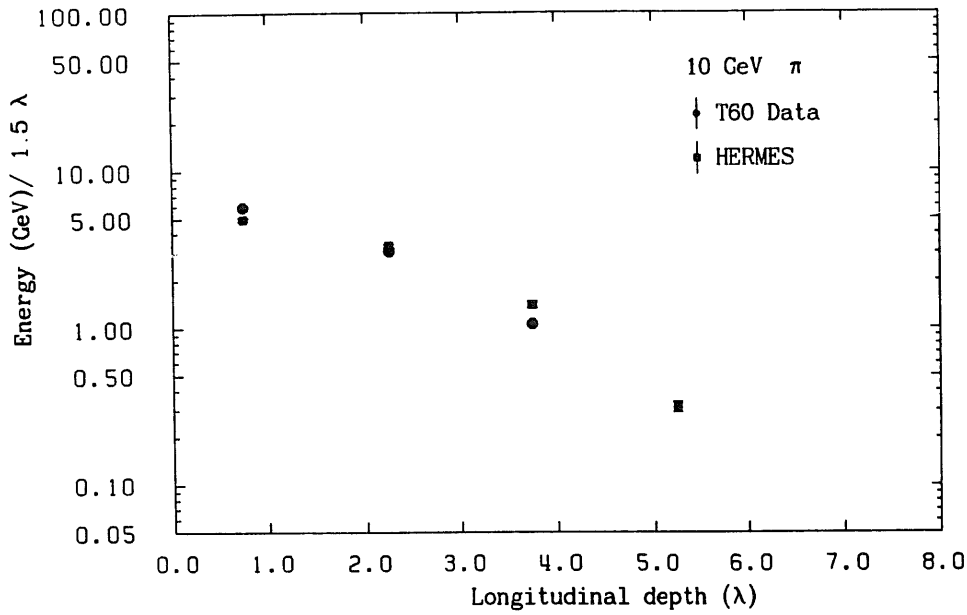

Fig. 3. (c) Longitudinal profiles for hadron showers measured at 10 GeV together with expectations in HERMES.

shower components. We are going to compare our data to two of those codes, namely

- NEUKA, and
- HERMES.

The basic ingredients of both Monte Carlo models are described in the following subsections.

The attenuation length of the plastic scintillator (~ 100 cm), as well as photostatistics effects in the photomultipliers (1.5 photoelectrons/MeV), were taken into account in this simulations. The geometry of the calorimeter modules described in the previous sections was fully incorporated. The beam spot was considered to be Gaussian distributed around the center of strip #7, where the hadron beam was chosen to impinge, with $\sigma_{ms} = 1$ cm. The leakage cut used in module #5 corresponds to the one used for the experimental analysis of the energy resolution [3].

3.1. NEUKA

NEUKA is based on the FLUKA code [15] for the simulation of high-energy hadron showers, including a

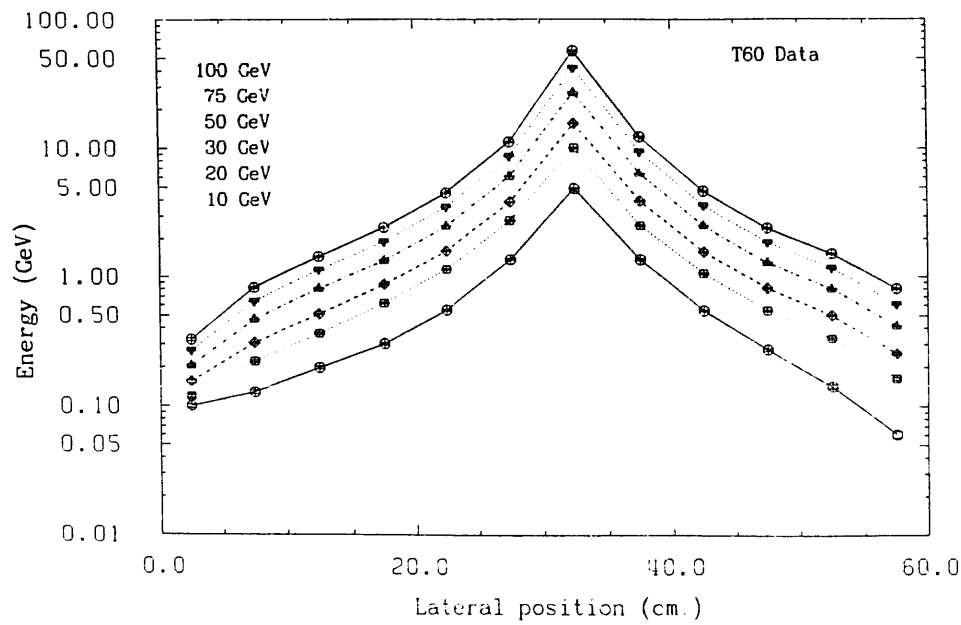

Fig. 4. (a) Transverse profiles, integrated over the whole calorimeter depth, for hadronic showers measured at 10, 20, 30, 50, 75, 100 GeV. The lines are meant to guide the eye.

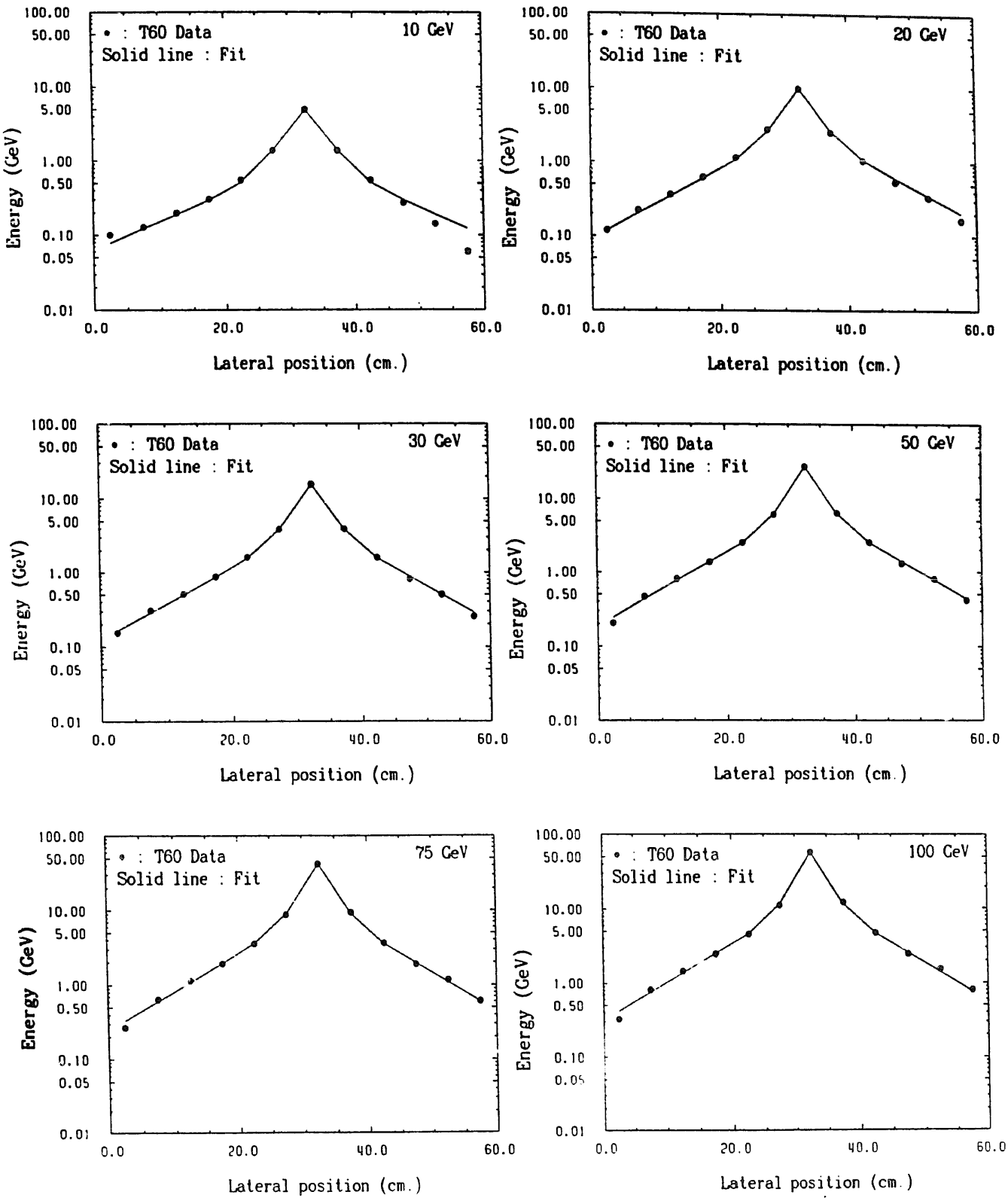

Fig. 4. (b) Transverse profiles, integrated over the whole calorimeter depth, for hadronic showers measured at 10, 20, 30, 50, 75 and 100 GeV along with the results of fits using eq. (8) (solid line).

description of hadronic cross sections and models for high-energy hadron–nucleus interactions. Because of the importance of the low-energy neutron component for the compensating properties of DU/Sci calorimeters particular emphasis have been devoted in NEUKA to production and interaction of evaporation neutrons. So

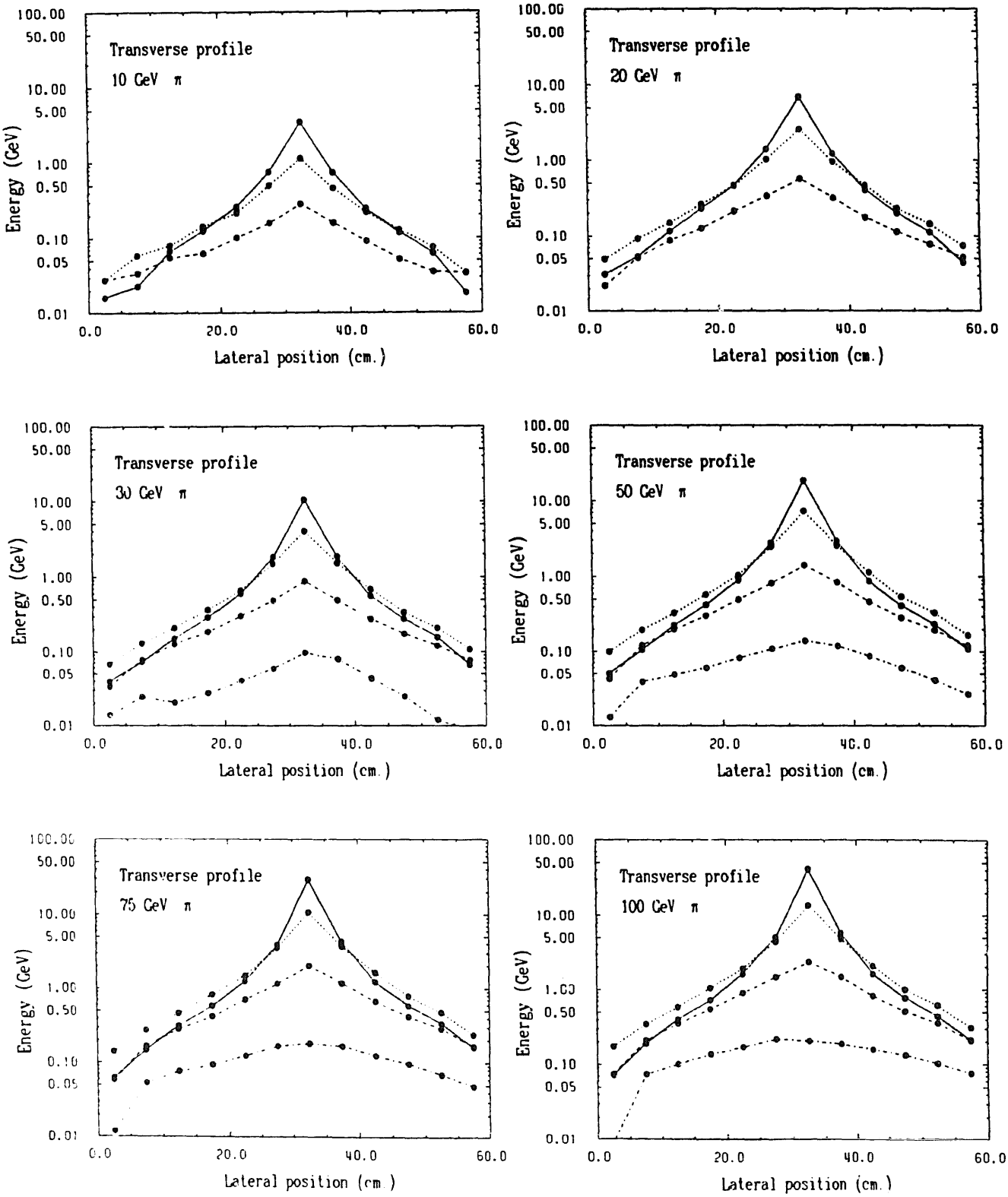

Fig. 5. Transverse profiles, as a function of calorimeter depth, for hadronic showers measured at 10, 20, 30, 50, 75 and 100 GeV. The solid line represents the first module, the dotted line the second, the dashed line the third and the dash-dotted line the fourth module. Each module is approximately 1.5λ deep.

far this shower component is not treated in any detail in the standard FLUKA version.

In order to save computing time the electromagnetic part of the cascade is not tracked but the energy deposition parametrized according to approximate analytical expressions for the average longitudinal and transverse

development of e/γ showers. This may be justified for the present study, since the spatial resolution of the energy deposition in the calorimeter is coarse as compared to the shape of typical electromagnetic showers. Note that NEUKA may also be coupled to the EGS code for the description of electromagnetic showers.

In the following the briefly discuss each of these components.

In the FLUKA code hadron–nucleus interactions are treated approximately as incoherent superposition of three processes:

- Multiparticle production of mostly relativistic secondaries; these processes are described via resonance production mechanisms at projectile energies below 5 GeV [32], and by a multichain fragmentation model [17] above that energy.
- Generation of protons and neutrons from intranuclear cascade processes, i.e. in the energy range from about 20 MeV up to potentially several hundred MeV; energy and angular distributions of those nucleons are generated according to empirical expressions, adjusted to describe particle fluxes at large angles with respect to the incident beam [16,32].
- Nuclear processes within the residual, generally highly excited nucleus like nuclear breakup, neutron evaporation, deexcitation by photon emission etc. In the FLUKA model these processes are not described in any detail but rather taken into account globally by assigning an "excitation" energy E_{exc} to the sum of these processes.

In NEUKA a certain fraction f_{exc} of that "excitation" energy is used as input to a neutron evaporation model [18], to initiate the low-energy neutron component of the shower. In that approach the mean number of neutrons evaporated in a single hadron–nucleus collision with given "excitation" energy E_{exc} is given by

$$\bar{n}_{evap} = \frac{f_{exc} E_{exc}}{\bar{E}_B + \bar{E}_n}, \quad (1)$$

where

- $\bar{E}_B$ denotes the average neutron binding energy, taken to be 6.4 MeV, which is the binding energy of outer shell neutrons in uranium;
- $\bar{E}_n$ denotes the average neutron kinetic energy, taken to be 3.5 MeV.

The value of the parameter f_{exc} was adjusted so that NEUKA correctly described the number of captured neutrons, measured from a 591 MeV proton beam incident on a DU/Sci calorimeter [19]. The value is $f_{exc} = 0.6 \pm 0.1$.

Table 1
Parameters used in the HERMES simulation

HETC	Transport energy cutoff p	1 MeV
	n	14.9 MeV
	μ	2.23 MeV
	π	1.69 MeV
	n, p elastic scattering	($K_B = 8.5 \times 10^{-3}$)
	isotropic evaporation	
	high energy fusion	
MORSE	100 neutron energy groups	10^{-4} eV to 14.9 MeV
	21 γ energy groups	0.1 to 14 MeV
	time cutoff	100 ns
	fission allowed	
NDEM	Troubetzkoy model	
	16 γ energy groups	0.5 to 8 MeV
PEGS4	AE	0.711 MeV
EGS4	AP	0.1 MeV
	ECUT	1.511 MeV
	PCUT	0.1 MeV
	ESTEPE	0.005 for U
		0.01 for Fe and Sc

Table 2
Longitudinal profiles in the range 10–100 GeV fully contained in the calorimeter (the 1st error is statistical and the 2nd systematic)

Depth (λ)	Data	NEUKA
(i) Energy deposited (GeV) for 10 GeV		
1.5	$5.890 \pm 0.039 \pm 0.088$	5.676 ± 0.116
3.0	$3.040 \pm 0.032 \pm 0.023$	3.166 ± 0.096
4.5	$1.089 \pm 0.020 \pm 0.034$	0.973 ± 0.061
(ii) Energy deposited (GeV) for 20 GeV		
1.5	$11.143 \pm 0.056 \pm 0.081$	10.457 ± 0.360
3.0	$6.457 \pm 0.043 \pm 0.020$	6.743 ± 0.300
4.5	$2.129 \pm 0.025 \pm 0.015$	2.347 ± 0.201
6.0	$0.282 \pm 0.008 \pm 0.113$	0.433 ± 0.089
(iii) Energy deposited (GeV) for 30 GeV		
1.5	$16.448 \pm 0.059 \pm 0.065$	15.990 ± 0.460
3.0	$9.866 \pm 0.045 \pm 0.042$	9.635 ± 0.325
4.5	$3.247 \pm 0.025 \pm 0.028$	3.713 ± 0.249
6.0	$0.450 \pm 0.007 \pm 0.112$	0.624 ± 0.040
(iv) Energy deposited (GeV) for 50 GeV		
1.5	$27.290 \pm 0.109 \pm 0.136$	25.178 ± 0.898
3.0	$16.638 \pm 0.083 \pm 0.097$	17.845 ± 0.755
4.5	$5.260 \pm 0.039 \pm 0.073$	5.689 ± 0.339
6.0	$0.824 \pm 0.010 \pm 0.110$	1.229 ± 0.081
(v) Energy deposited (GeV) for 75 GeV		
1.5	$42.120 \pm 0.199 \pm 0.239$	40.742 ± 1.579
3.0	$24.185 \pm 0.149 \pm 0.143$	25.149 ± 1.392
4.5	$7.502 \pm 0.066 \pm 0.100$	7.444 ± 0.407
6.0	$1.208 \pm 0.014 \pm 0.113$	1.567 ± 0.109
(vi) Energy deposited (GeV) for 100 GeV		
1.5	$58.145 \pm 0.380 \pm 0.247$	51.780 ± 2.698
3.0	$31.000 \pm 0.278 \pm 0.169$	33.892 ± 2.045
4.5	$9.283 \pm 0.105 \pm 0.121$	11.826 ± 0.754
6.0	$1.583 \pm 0.027 \pm 0.109$	2.357 ± 0.181

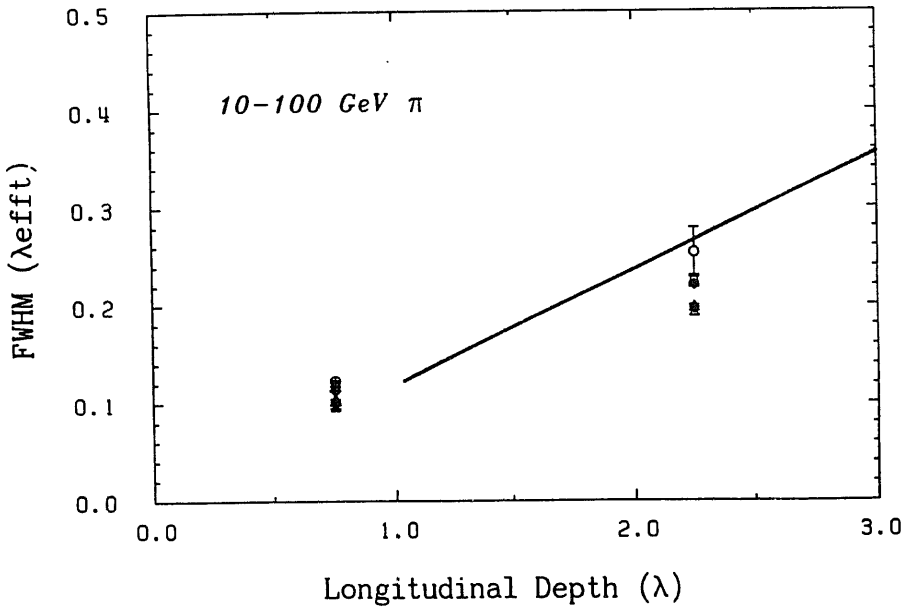

Fig. 6. The full width at half maximum for the central "core" of hadronic showers measured at 10, 20, 30, 50, 75 and 100 GeV. The solid line is taken from [27].

Each neutron generated with a kinetic energy below 20 MeV is transferred to a Neutron Monte Carlo designed particularly for the description of those neutron–nucleus processes which are assumed to dominate transport and energy deposition in DU/Sci calorimeters, see [18]. In our simulation the cutoff for neutron transport was chosen to be 1 keV. With the help of this code, the neutron sampling fraction, α_n, is estimated as a function of the absorber and scintillator thicknesses. The neutron sampling fraction α_n is defined as that fraction of the energy devoted to the generation of low-energy neutrons, i.e. with $E_{kin} < 20$ MeV, which is converted into a signal in the scintillator.

The electromagnetic energy deposition is simulated according to a simple parametrization [15,9] with a factorized description of the longitudinal and lateral shower developments. The radial distribution of the energy deposited by photons or electrons is approximated by

$$f(r) = 1.1\exp(-2.28r) + \exp(-0.635r), \quad (2)$$

where r is expressed in Molière units.

The average longitudinal shower shape is taken from fits to EGS calculations [31]

$$f(z) = z^a \exp(-bz), \quad (3)$$

with

$$a = 2.0 - Z/340 + (0.664 - Z/340)\ln(E),$$

$$b = 0.634 - 0.0021Z;$$

Z is the atomic number of the material, E is the photon or electron energy in GeV and z is the distance to the shower vertex in units of radiation lengths.

To obtain the signal due to the electromagnetic component, the energy deposition from the above parametrization is "smeared" (in energy) with the measured electromagnetic resolution $\sigma_{ele} = 15\%\sqrt{E_{ele}}$ [3], and multiplied by the sampling fraction α_{ch} for minimum ionizing particles as well as by the e/mip ratio.

Thus the total signal S for a given hadron shower is given by the sum

$$S = S_{ch} + \frac{e}{mip}\alpha_{ch}E_{ele} + \alpha_n\bar{E}_n\frac{f_{exc}E_{exc}^{tot}}{\bar{E}_n + \bar{E}_B}, \quad (4)$$

where E_{exc}^{tot} denotes the sum of "excitation" energies from all hadron–nucleus interactions in the given shower.

Let us finally remark that the generation of a 10 GeV hadronic shower needs about 20 s CPU time on an IBM 3084Q.

3.2. HERMES

The HERMES (High Energy Radiation Monte Carlo Elaborate System) code [10,11] is a collection of Monte Carlo computer programs which are run separately and exchange particle information through data files.

The hadronic part of the cascade is simulated with the HETC (High Energy Transport Code) Monte Carlo program [20] based on the Intra Nuclear Cascade Evaporation model (INCE). The HETC code transports neutrons, protons, pions, muons and light ions (up to $A = 20$). The neutrons with an energy below the transport energy cutoff (see table 1) are passed to the MORSE Monte Carlo [21], which tracks them down to thermal energies. It also takes into account the gammas generated in (n, γ) reactions. The deexcitation of the residual

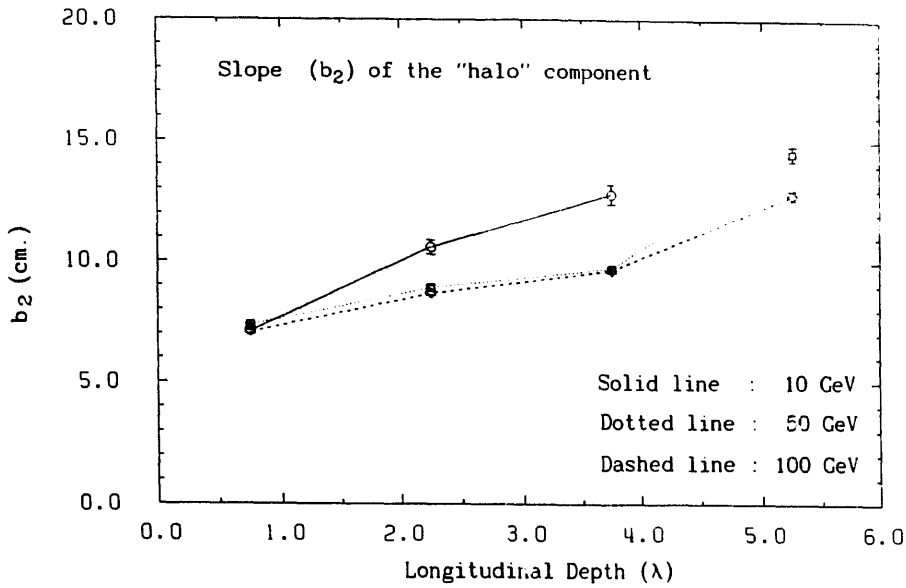

Fig. 7. The slope of the halo component for hadronic showers measured at 10, 50 and 100 GeV, as a function of calorimeter depth. The lines are meant to guide the eye.

nuclei after the intranuclear cascade is treated by the NDEM Monte Carlo. This deexcitation generates gammas. This part of the cascade was not simulated in the NEUKA code. The electromagnetic part of the cascade is simulated with the EGS4 code [24]. In the HERMES system, not only the π^0's and $e^{\pm}$'s produced in HETC are treated by EGS4, but also the γ's from MORSE ((n, γ) reactions) and from NDEM (deexcitation). The parameters used in our simulation are summarized in table 1.

HERMES is much more time consuming than NEUKA, because the electromagnetic energy deposition and the neutron transport is done accurately. Some parts, essentially describing particle production in hadron nucleus collisions, are however based on assumptions which are only valid at low energies, say below 5–10 GeV. On the other hand, NEUKA is supposed to be valid at higher energies and is much less CPU time consuming, at the expense of having the electromagnetic energy deposition based on global parametrizations and a somewhat simplified model for the low-energy neutron component.

Finally we would like to stress that the Monte Carlo calculations have been carried out with the standard versions of both the mentioned codes, i.e. without additional tuning of model parameters according to the conditions of our experiment.

4. Results

4.1. Electromagnetic showers

Before embarking upon a discussion on data for hadronic showers we would like to mention that electromagnetic showers are very well reproduced by the EGS code. For instance we find experimentally that showers initiated by 10 GeV electrons are essentially contained in the first module and deposit 91.6% of their energy in the strip upon which the beam is impinging, while 4% is collected at each of the two adjacent strips, see [22] for a similar lead scintillator calorimeter. These results are little dependent on incident energy and well reproduced by a simulation of electromagnetic showers in a geometry like that in our experimental setup as implemented in the package GEANT3 [25]. For the sake of completeness we note that according to these simulations the predicted energy deposited in the central strip was 91.3% and 4.1% in the adjacent strip. We do not consider this agreement as a significant test of the EGS code used in GEANT, but rather as a check that we understand our experiment.

4.2. Longitudinal profiles

We start by showing in fig. 3a the longitudinal profiles for hadronic showers measured at energies of 10, 20, 30, 50, 75 and 100 GeV (full symbols). The profiles have always been normalized to the nominal incident energy. Notice that these data are obtained by relaxing the cut on the energy deposited in the fifth module, therefore assuming that the shower is fully contained in the calorimeter which is 7.1λ deep. In spite of the problem with the absolute normalization, we present these data for the sake of comparison with the WA78 Collaboration which has recently measured longitudinal profiles for hadronic showers in this energy range [26], with a calorimeter which is 13λ and segmented in depth every 0.45λ. They have fitted their data to an analytical expression for the development of

Table 3
Lateral profiles in the range 10–100 GeV (the 1st error is statistical and the 2nd systematic)

(i) Energy deposited (GeV) for 10 GeV

Strip	Data	NEUKA	HERMES	GEANT (GHEISHA)
1	0.100 ± 0.003 ± 0.020	0.054 ± 0.004	0.065 ± 0.006	0.045 ± 0.003
2	0.128 ± 0.004 ± 0.019	0.081 ± 0.005	0.119 ± 0.008	0.085 ± 0.004
3	0.199 ± 0.005 ± 0.019	0.139 ± 0.007	0.183 ± 0.011	0.153 ± 0.006
4	0.305 ± 0.006 ± 0.026	0.250 ± 0.011	0.267 ± 0.012	0.259 ± 0.008
5	0.553 ± 0.009 ± 0.012	0.494 ± 0.019	0.531 ± 0.021	0.489 ± 0.011
6	1.379 ± 0.017 ± 0.020	1.212 ± 0.040	1.352 ± 0.047	1.236 ± 0.024
7	4.938 ± 0.046 ± 0.102	5.565 ± 0.149	4.965 ± 0.132	5.618 ± 0.095
8	1.375 ± 0.017 ± 0.020	1.248 ± 0.044	1.346 ± 0.048	1.159 ± 0.024
9	0.548 ± 0.009 ± 0.012	0.485 ± 0.018	0.566 ± 0.023	0.470 ± 0.011
10	0.273 ± 0.006 ± 0.026	0.249 ± 0.012	0.326 ± 0.017	0.262 ± 0.008
11	0.141 ± 0.005 ± 0.019	0.140 ± 0.007	0.180 ± 0.010	0.151 ± 0.006
12	0.060 ± 0.003 ± 0.019	0.083 ± 0.006	0.100 ± 0.007	0.075 ± 0.004

Strip	Data
(ii) Energy deposited (GeV) for 20 GeV	
1	0.119 ± 0.003 ± 0.020
2	0.221 ± 0.004 ± 0.018
3	0.365 ± 0.005 ± 0.020
4	0.626 ± 0.006 ± 0.026
5	1.148 ± 0.010 ± 0.013
6	2.779 ± 0.020 ± 0.017
7	10.085 ± 0.068 ± 0.112
8	2.546 ± 0.019 ± 0.017
9	1.067 ± 0.009 ± 0.013
10	0.547 ± 0.006 ± 0.026
11	0.332 ± 0.005 ± 0.020
12	0.164 ± 0.003 ± 0.018
(iii) Energy deposited (GeV) for 30 GeV	
1	0.154 ± 0.004 ± 0.019
2	0.308 ± 0.004 ± 0.019
3	0.513 ± 0.004 ± 0.020
4	0.873 ± 0.006 ± 0.026
5	1.610 ± 0.009 ± 0.014
6	3.871 ± 0.018 ± 0.018
7	15.570 ± 0.072 ± 0.114
8	3.944 ± 0.019 ± 0.018
9	1.584 ± 0.009 ± 0.014
10	0.816 ± 0.006 ± 0.026
11	0.501 ± 0.004 ± 0.020
12	0.256 ± 0.003 ± 0.019
(iv) Energy deposited (GeV) for 50 GeV	
1	0.205 ± 0.004 ± 0.019
2	0.465 ± 0.005 ± 0.019
3	0.807 ± 0.006 ± 0.019
4	1.357 ± 0.008 ± 0.026
5	2.513 ± 0.013 ± 0.012
6	6.113 ± 0.029 ± 0.018
7	27.062 ± 0.135 ± 0.104
8	6.418 ± 0.031 ± 0.018
9	2.539 ± 0.013 ± 0.012
10	1.299 ± 0.008 ± 0.026
11	0.804 ± 0.006 ± 0.019
12	0.418 ± 0.004 ± 0.019

Strip	Data
(v) Energy deposited (GeV) for 75 GeV	
1	0.267 ± 0.004 ± 0.019
2	0.642 ± 0.006 ± 0.019
3	1.136 ± 0.008 ± 0.019
4	1.909 ± 0.012 ± 0.026
5	3.560 ± 0.020 ± 0.013
6	8.740 ± 0.046 ± 0.021
7	41.974 ± 0.245 ± 0.085
8	9.449 ± 0.051 ± 0.021
9	3.656 ± 0.021 ± 0.013
10	1.885 ± 0.012 ± 0.026
11	1.173 ± 0.008 ± 0.019
12	0.610 ± 0.005 ± 0.019
(vi) Energy deposited (GeV) for 100 GeV	
1	0.325 ± 0.007 ± 0.020
2	0.821 ± 0.010 ± 0.019
3	1.454 ± 0.013 ± 0.019
4	2.460 ± 0.020 ± 0.026
5	4.556 ± 0.035 ± 0.014
6	11.225 ± 0.079 ± 0.018
7	57.327 ± 0.464 ± 0.103
8	12.340 ± 0.092 ± 0.018
9	4.720 ± 0.037 ± 0.014
10	2.434 ± 0.020 ± 0.026
11	1.530 ± 0.014 ± 0.019
12	0.809 ± 0.008 ± 0.019

Table 4
Fits to hadronic transverse profile

	10 GeV	20 GeV	30 GeV	50 GeV	75 GeV	100 GeV
A_1	6.8 ±0.1	14.5 ±0.2	23.2 ±0.2	42.9 ±0.4	69.9 ±0.7	99. ±1.
b_1	1.96±0.04	1.55±0.02	1.50±0.01	1.39±0.01	1.31±0.01	1.25±0.02
A_2	1.11±0.04	3.08±0.05	4.57±0.05	7.64±0.01	11.4 ±0.1	15.0 ±0.2
b_2	11.3 ±0.3	9.14±0.08	8.99±0.05	8.68±0.01	8.47±0.04	8.35±0.04

hadronic showers. The energy deposited dE/dx as a function of the distance x from the shower vertex can be parametrized as the sum of two terms describing the electromagnetic [23] and hadronic component of the shower

$$\frac{dE}{dx} = E\left\{\alpha\frac{b^{a+1}}{\Gamma(a+1)}x^a \exp(-bx) + (1-\alpha)c\exp(-cx)\right\}. \quad (5)$$

In order to describe the longitudinal shower profile, measured from the front end of the calorimeter (t), one ought to convolute the energy deposition given above, eq. (5), with the probability of the beam particle to shower at a given depth (x) in the calorimeter, namely,

$$\frac{dE}{dt} = \frac{1}{\lambda_\pi}\int_0^t \exp\left(-\frac{x}{\lambda_\pi}\right)\frac{dE}{dx}(t-x)\,dx, \quad (6)$$

where $\lambda_\pi = 1.11$ is the interaction length of the incoming hadrons in units of the nominal interaction length.

The WA78 Collaboration finds that the above expressions with $\alpha = 0.13 \pm 0.02$, $a = 3$, $b = 19.5$ and furthermore

$$c(\lambda_{\text{int}}^{-1}) = (0.67 \pm 0.03) - (0.166 \pm 0.003)\ln\left(\frac{E\ [\text{GeV}]}{50.0}\right) \quad (7)$$

give a good representation of their data for energies above 10 GeV. This is qualitatively also true for our data as can be seen from fig. 3a, where the solid lines are taken from [26]. We remark however that while the agreement between our data and the WA78 parametrization is fair in the first half of the spectrum, our experimental points lie systematically below the curves for depths beyond 5λ. It is interesting to note that the WA78 calorimeter is composed of two parts, a depleted uranium section and an iron section, the transition between both taking place at 5.4λ. We also point out that due to our coarse segmentation we are not in a position to make independent fits from our data to the parametrizations discussed above, for we are not sensitive to the development of the electromagnetic part.

In order to ensure full containment of the shower in the calorimeter, we will use from now on the fifth module as a veto calorimeter as discussed in section 2. The Monte Carlo data will be subject to the same constraint. We show in fig. 3b the longitudinal profiles for hadron showers measured at energies of 10, 20, 30, 50, 75 and 100 GeV (full symbols) compared with the expectations in NEUKA [9], open symbols. The overall agreement is good though some deviations between data and Monte Carlo are seen in particular above 5λ. In fig. 3c, we compare the longitudinal profile for a 10 GeV hadronic shower which is fully contained in the calorimeter, with the HERMES predictions. The same trend as discussed above is here observed. For the sake of completeness the comparison with NEUKA is presented in table 2. Systematic errors affecting the data have been obtained by taking into account the uncertainties due to the pedestals determination. Two additional comments are in order:

- We would like to point out that a comparison with HERMES at energies above 10 GeV is precluded for reasons discussed in the previous section.
- it has been shown previously that current Monte Carlos for hadronic showers [9] are able to describe longitudinal profiles finely segmented in depth as measured by the WA78 Collaboration [26].

4.3. Transverse profiles

The transverse shower profiles measured at the same six energies as above are presented in table 3 and displayed in fig. 4a. The systematic errors affecting the data and given in table 3 reflect the uncertainties discussed above. The solid lines in fig. 4a are drawn to guide the eye. This figure indicates the presence of two distinct components, namely a sharp central "core" on top of a "halo" of low-energetic particles extending to distances of $\mathcal{O}(2\lambda)$. We try to describe the transverse profiles, in rectangular coordinates of the calorimeter, by the sum of two exponentials, which are supposed to describe the central "core" of the shower and its "halo":

$$f(x) = A_1\exp\left(-\left|\frac{x-x_0}{b_1}\right|\right) + A_2\exp\left(-\left|\frac{x-x_0}{b_2}\right|\right), \quad (8)$$

with x the transverse coordinate in cm and x_0 the impact point of the showers.

Table 5
Fits to hadronic transverse profile by modules

	10 GeV	20 GeV	30 GeV	50 GeV	75 GeV	100 GeV
A_1	5.6 ±0.1	11.9 ±0.2	18.9 ±0.2	34.5 ±0.3	58.2 ±0.6	85.0 ±1.0
b_1	1.37 ±0.03	1.36±0.02	1.33 ±0.01	1.24 ±0.01	1.19 ±0.01	1.15 ±0.01
A_2	0.98 ±0.03	1.53±0.03	2.06 ±0.03	3.27 ±0.04	4.79 ±0.07	6.4 ±0.1
b_2	7.1 ±0.1	7.58±0.07	7.58 ±0.05	7.35 ±0.04	7.18 ±0.04	7.06 ±0.06
A_1	1.1 ±0.1	2.5 ±0.1	4.1 ±0.1	8.1 ±0.2	11.9 ±0.3	15.4 ±0.6
b_1	2.2 ±0.2	1.98±0.09	2.00 ±0.05	1.88 ±0.04	1.85 ±0.04	1.81 ±0.06
A_2	0.53 ±0.03	1.23±0.04	1.85 ±0.03	3.05 ±0.05	4.48 ±0.07	5.9 ±0.1
b_2	10.6 ±0.3	9.3 ±0.1	9.15 ±0.08	8.91 ±0.07	8.76 ±0.06	8.67 ±0.08
A_1	0.216±0.007	0.53±0.01	0.789±0.009	1.38 ±0.01	1.99 ±0.02	2.50 ±0.04
b_1	12.8 ±0.4	10.0 ±0.1	10.4 ±0.1	9.74 ±0.07	9.64 ±0.07	9.66 ±0.09
A_1	–	–	0.099±0.003	0.164±0.003	0.256±0.005	0.350±0.008
b_1	–	–	12.7 ±0.4	14.5 ±0.3	14.2 ±0.3	12.8 ±0.2

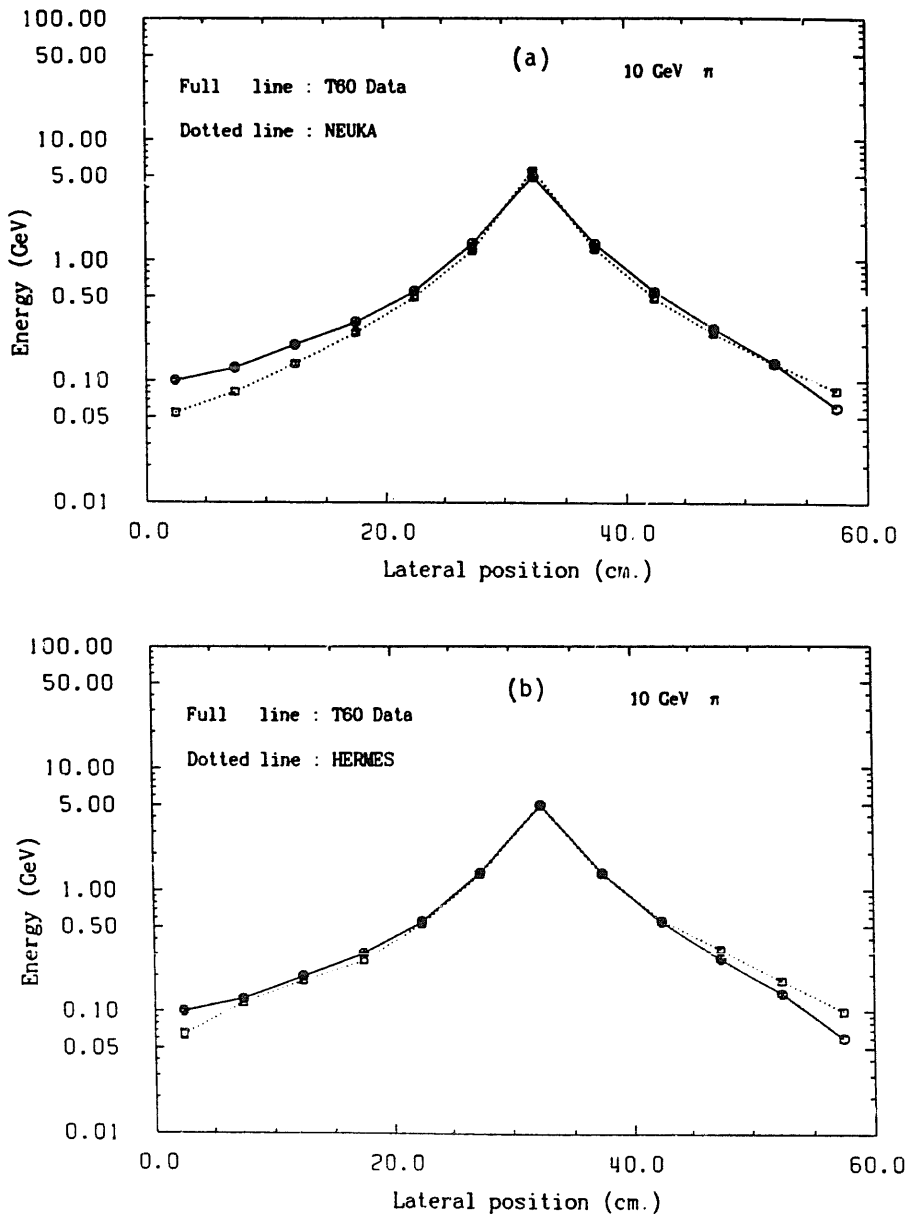

Fig. 8. (a) Transverse profile of a 10 GeV hadronic shower along with the expectation in NEUKA. (b) Transverse profile of a 10 GeV hadronic shower along with the expectation in HERMES.

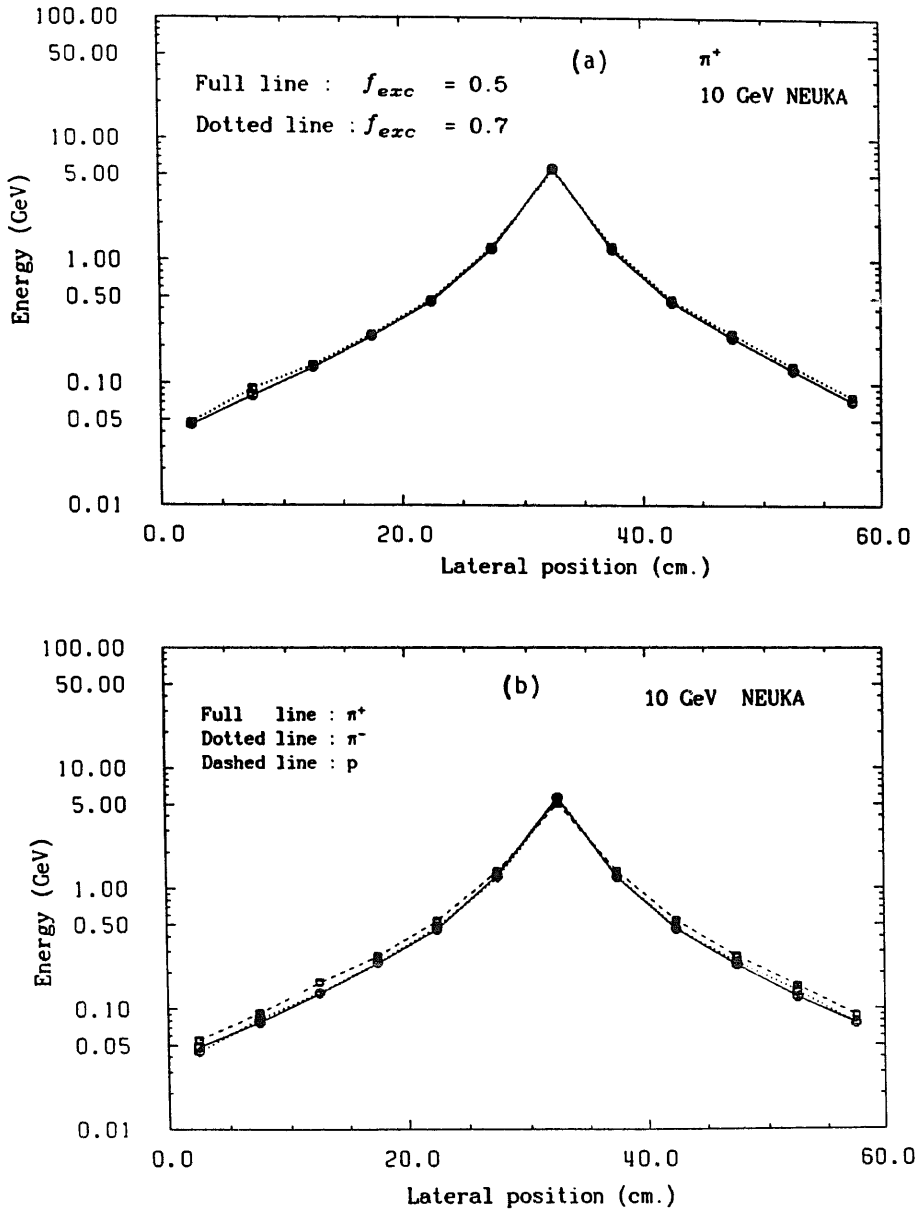

Fig. 9. (a) Transverse profiles for 10 GeV charged pions in NEUKA for different values of the number of evaporated neutrons f_{exc}. This parameter has been allowed to vary between the lower and upper limits imposed by requirements on the total energy resolution. (b) Transverse profiles for 10 GeV π^+, π^- and p in NEUKA.

The data in fig. 4a have been fitted to the expression given above taking b_1, b_2 and A_1, and A_2 as free parameters. For the sake of illustration we show in fig. 4b a comparison between our data in the range of 10 to 100 GeV and the fit results. The values obtained for b_i and A_i are given in table 4. Notice that while the normalization factors increase with the energy, the slopes tend to decrease very slowly with increasing energy.

In order to see how the slower transverse dimensions evolve as a function of depth in the calorimeter, we show in fig. 5 the transverse profile of the shower for each energy and for separate calorimeter modules (excluding the fifth one, which was used as a veto calorimeter).

Fig. 6 illustrates the dependence of the "Full Width at Half Maximum" (FWHM) of the transverse profile with the depth in the calorimeter, at the six energies under study. It is given by $2|x_h - x_0|$ with x_h such that $f(x_h) = f(x_0)/2$, $f(x)$ being given by eq. (8). It has been shown that if the FWHM is given in units of interaction lengths (λ), this dependence exhibits a linear and scaling behaviour up to depths of $\mathcal{O}(4\lambda)$ [27]. The solid line in fig. 6 is supposed to represent marble [28], iron [29] and wolfram [30] data. We can compare

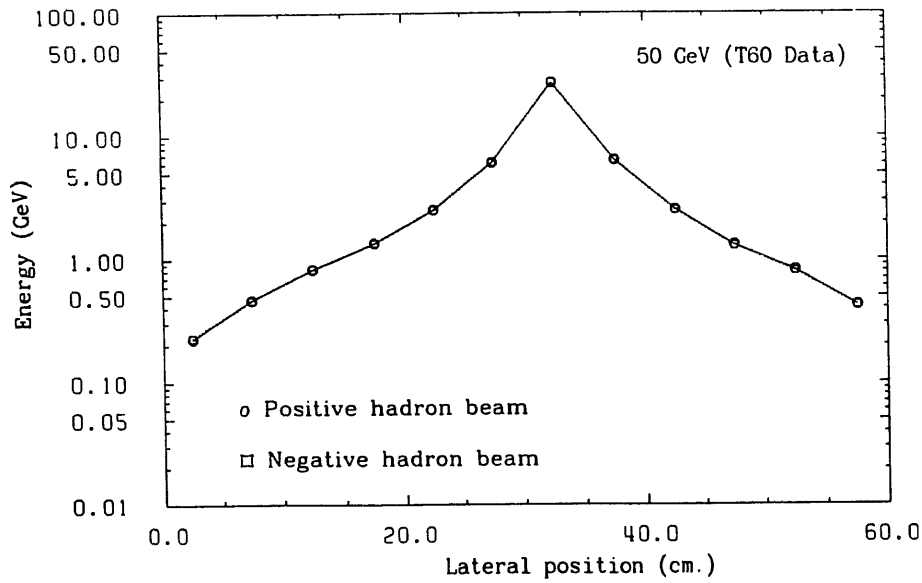

Fig. 10. Transverse profiles for 50 GeV opposite charge hadron showers measured by TEST60.

our results with those from [27] only for those modules where the central "core" has not faded away: these are modules #1 and #2 as can be seen in fig. 5. For these depths the agreement is good.

The functional dependence given by eq. (8), found to describe the transverse profiles shown in fig. 4a, gives also an adequate description of the partial transverse profiles shown in fig. 5 for the first two modules, where the central "core" is still present. In the last two modules, the contribution due to the "halo" suffices to explain our data. The results of the corresponding fits are presented in table 5.

The slopes associated with the two components of the shower decrease very slowly with increasing energy, and grow with shower depth, see fig. 7, where b_2 is shown as a function of λ for three energies 10, 50 and 100 GeV. This is a reflection of the fact that as the shower propagates into the calorimeter it becomes broader.

In order to see how well these data on transverse profiles are reproduced by the two Monte Carlo codes discussed in a previous section, we plot in fig. 8a and 8b the transverse profile for a hadronic shower initiated by a 10 GeV positive hadron beam along with the expectations for 10 GeV charged pions in NEUKA and HERMES. Both Monte Carlo codes describe the gross features of the data although NEUKA seems to give rise to profiles which are slightly narrower than the experimental data.

It is interesting to investigate the uncertainties affecting the Monte Carlo calculations performed so far, caused by the fraction of evaporated neutrons and the composition of the beam. In fig. 9a we present the results of a NEUKA simulation of 10 GeV showers initiated by charged pions for two values of the parameter f_{exc}, namely 0.5 to 0.7. These values bracket the allowed range of variation of f_{exc} at the 1σ level. Though the profile corresponding to the latter value is broader, the differences are almost negligible. In fig. 9b, we present the results of a simulation with NEUKA of transverse profiles for 10 GeV showers initiated by π^+, π^- and protons. We learn that oppositely charged pions give rise to very similar lateral profiles, while protons are just slightly broader.

We would like to remark that the NEUKA prediction about the equality of transverse profiles for oppositely charged particles is supported by our data. This is shown in fig. 10 where we present measurements for the transverse profiles initiated by 50 GeV oppositely charged hadron beams.

In order to gain further insight into the transverse energy deposition in a hadronic shower, we plot in fig. 11 the Monte Carlo predictions given by HERMES and NAUKA for the shape of the profiles for the three main components that we discussed above. It is clearly seen that while the ionization and electromagnetic components are responsible for the central "core", the contribution of the neutron signal is very important to describe the tails. Thus, in order to describe the transverse profiles of hadronic cascades, a Monte Carlo with accurate description of low-energetic neutrons is required. We also would like to point out that both codes HERMES and NEUKA give very similar predictions for the three different shower components in spite of the fact that they are based on very different treatments.

In order to further illustrate this point we shown in fig. 12 a comparison between our data for transverse profiles initiated by 10 GeV positive hadron beams and the results of a simulation within the GEANT package

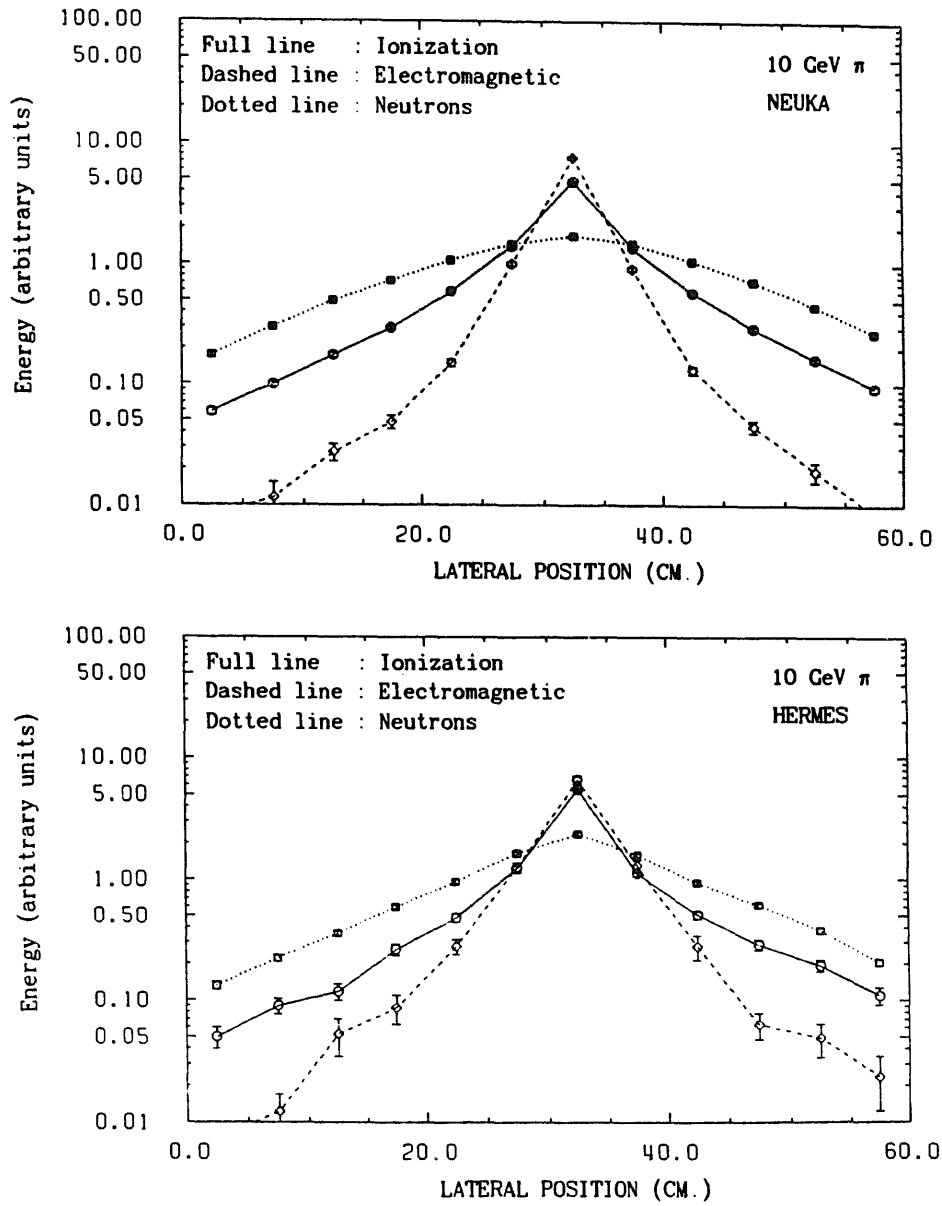

Fig. 11. The lateral profile of the three components contributing to a hadronic shower as predicted by HERMES and NEUKA in arbitrary units.

[25], version 3.12, implementing two different hadron shower treatments, i.e. TATINA and version 7.3 of GHEISHA [33]. Clearly the transverse profiles in TATINA, where the neutron component is missing, are much narrower than those in NEUKA/HERMES/GHEISHA and in turn than in the data.

We would like to remark that for the ZEUS experiment a neutron shower termination program has been added to the GEANT package and tuned to the ZEUS prototype data [34]. This termination program significantly speeds up GEANT and simulates adequately the experimental spatial distributions, energy resolution and e/h ratios.

We would like to finish this section by noting that the transverse profiles we have been discussing in this section are rather insensitive to the 2% cut applied in the energy deposited in the fifth module. This is illustrated in fig. 13 where we show the transverse profiles for 100 GeV hadron showers with and without the leakage cut.

4.4. Influence of leakage on the energy resolution

The segmentation of our calorimeter in five modules in depth and twelve strips in the transverse dimensions allows an investigation on how leakage effects influence the energy resolution for hadronic showers [14].

To study this point we have measured the pulse height distributions in the full calorimeter, using the fifth module as a veto calorimeter, and have then

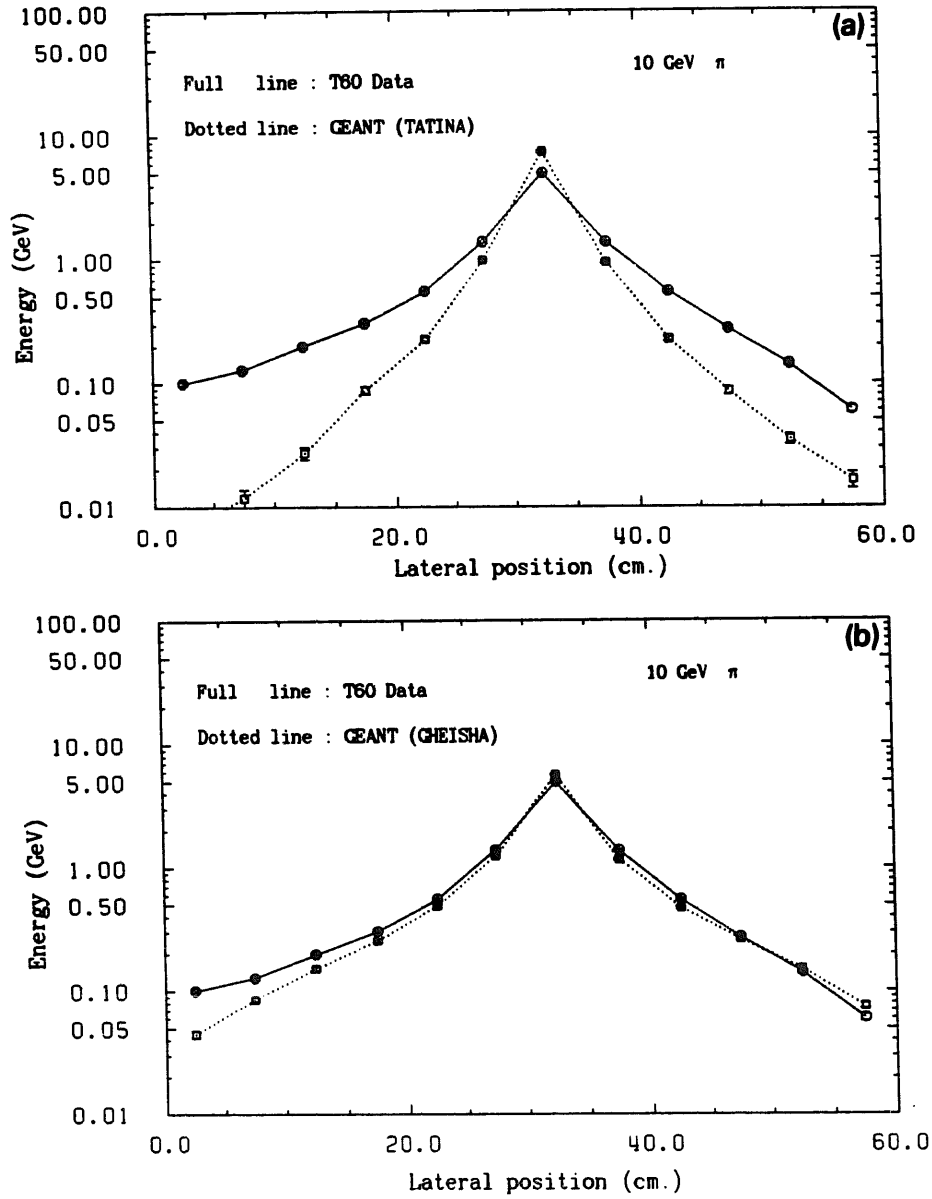

Fig. 12. Transverse profiles for a 10 GeV hadronic shower along with the expectations in TATINA (a), and GHEISHA (b).

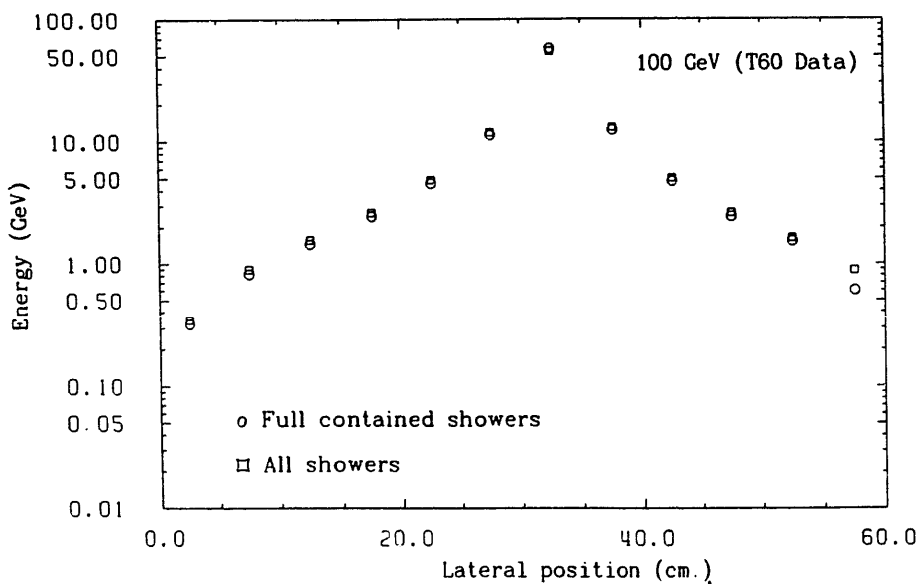

Fig. 13. Transverse profiles for a 100 GeV hadronic shower with and without longitudinal leakage cut.

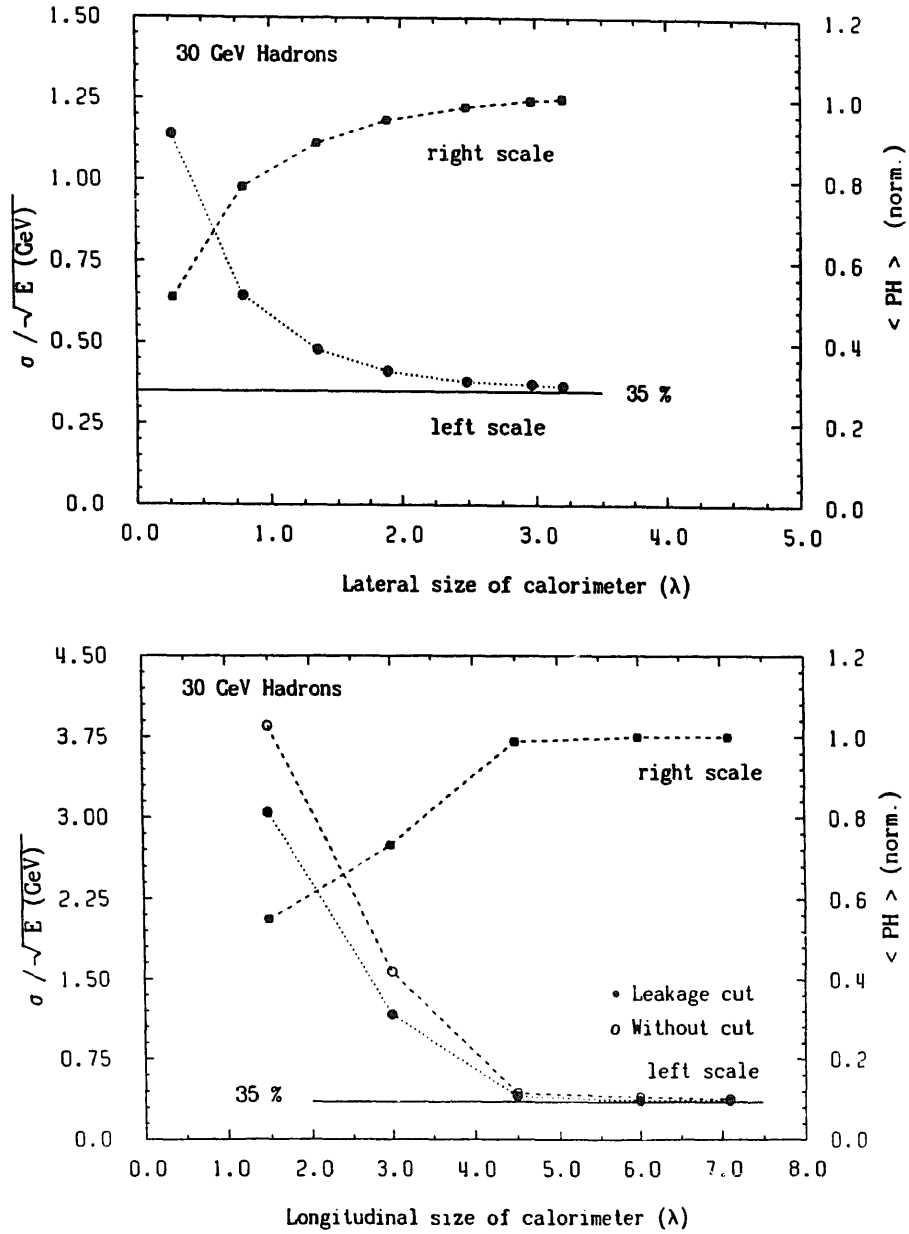

Fig. 14. The mean response, right scale, and the energy resolution, left scale, as a function of longitudinal and transverse dimensions of the calorimeter.

- increased the longitudinal leakage by reducing stepwise the number of modules that contribute to the signal;
- increased the transverse leakage by reducing the number of strips which contribute to the signal.

The corresponding pulse-height distributions have been fitted to Gaussians over an interval of ± 3 standard deviations around the peak, the mean value is quoted as mean response and the standard deviation is used to obtain the energy resolution. The results are summarized in fig. 14 as exemplified in the case of 30 GeV hadron showers. This figure shows how the final resolution of $36.6\%/\sqrt{E}$ is approached when the calorimeter tends to its final configuration. Clearly the longitudinal leakage affects the energy resolution much stronger than the transverse leakage.

5. Summary

We have presented data on the longitudinal and transverse profiles of hadronic initiated showers at energies of 10, 20, 30, 50, 75 and 100 GeV. The longitudinal profiles agree with those measured by other experiments and are fairly well reproduced by the Monte Carlo programs HERMES and NEUKA incorporating the development of hadronic cascades as well as a simulation of the detector effects.

The lateral profiles show the presence of two distinct components, a narrow central "core" and a "halo" of low energetic particles. The central "core" is mainly due to ionization energy losses and electromagnetic deposition while the "halo" is dominated by the neutron component. The Monte Carlo programs HERMES and NEUKA with accurate treatment of low-energetic neutrons give an adequate description of the data.

Finally we have performed a study which shows the influence of longitudinal and transverse leakage on the energy resolution of a hadron calorimeter.

Acknowledgements

We gratefully acknowledge the help of the workshops of the participating institutions, in particular of NIKHEF-H for the production of the calorimeter modules, DESY and University of Hamburg for the machining of the scintillator and the wavelength shifters, and the Universidad Autonoma de Madrid for the photomultiplier mountings. We are also grateful for the help given by the EA-group of CERN which made an efficient use of the test beam possible. The support given by J. Tuyn, C. Lamberet and G. Roubaud at CERN for the handling and transportation of the depleted uranium is very much appreciated. The members of the UAM thank the exchange program "Acciones Integradas", CICYT-Kfz Karlsruhe for funding short stays at DESY during which part of these studies were made. Last but not least we would like to thank G. Wolf for a critical reading of the manuscript and J. del Peso for helpful comments on the use of the GEANT package at DESY.

References

[1] The ZEUS Detector, Technical Proposal of the ZEUS Collaboration.
[2] B. Anders et al., DESY Report 86-105.
[3] G. d'Agostini et al., Nucl. Instr. and Meth. A274 (1989) 134.
[4] J.E. Brau and T.A. Gabriel, Nucl. Instr. and Meth. A238 (1985) 489.
[5] H. Brückmann et al., Nucl. Instr. and Meth. A263 (1988) 136.
[6] R. Wigmans, Nucl. Instr. and Meth. A259 (1987) 389.
[7] C.W. Fabjan et al., Nucl. Instr. and Meth. 141 (1977) 61.
[8] H. Tiecke, Nucl. Instr. and Meth. A277 (1989) 42.
[9] H. Kowalski, H.J. Möhring and T. Tymieniecka, DESY 87-170.
[10] P. Cloth, D. Filges, R.D. Neef, G. Sterzenbach, Ch. Reul, T.W. Armstrong, B.L. Colborn, B. Anders and H. Brückman, KFA-Jülich report 2203.
[11] B. Anders, P. Cloth, D. Filges, Ch. Reul and G. Sterzenbach, Nucl. Instr. and Meth. A277 (1989) 56.
[12] Product of KYOWA, Japan.
[13] Product of Polivar, Italy.
[14] E. Bernardi, Ph.D. Thesis, University of Hamburg (1984).
[15] FLUKA86 User's Guide, P.A. Aarnio, A. Fasso, H.-J. Moehring, J. Ranft and G.R. Stevenson, CERN, TIS-RP/168.
[16] J. Ranft and J.T. Routti, Part. Accel. 4 (1972) 101.
[17] J. Ranft and S. Ritter, Z. Phys. C27 (1985) 569.
[18] T. Tymieniecka, ZEUS-Note 88-018.
[19] C. Leroy, Y. Sirois and R. Wigmans, Nucl. Instr. and Meth. A252 (1986) 4.
[20] T.W. Armstrong and K.C. Chandler, Nucl. Sci. Eng. 49 (1972) 110.
[21] M.B. Emmett, ORNL-4972, Oak Ridge (February 1983).
[22] F. Barreiro et al., Nucl. Instr. and Meth. A257 (1987) 145.
[23] U. Amaldi, Phys. Scripta 23 (1981) 409.
[24] W.R. Nelson, H. Hirayama and D.W.O. Rogers, The EGS4 Code SLAC-265 (Dec. 1985).
[25] R. Brun et al., GEANT User Manual, CERN DD/EE/84-1 (September 1987).
[26] M.G. Catanesi et al., Nucl. Instr. and Meth. A260 (1987) 43.
[27] C.W. Fabjan, in: Experimental Techniques in High Energy Physics, ed. T. Ferbel.
[28] M. Jonker et al., Nucl. Instr. and Meth. 200 (1982) 183.
[29] M. Holder et al., Nucl. Instr. and Meth. 151 (1978) 69.
[30] D.L. Cheshire et al., Nucl. Instr. and Meth. 141 (1977) 219.
[31] Particle Data Group, M. Aguilar-Benitez et al., Review of Particle Properties, Phys. Lett. B170 (1986).
[32] K. Hänsgen, H.-J. Möhring and J. Ranft, Nucl. Sci. Eng. 88 (1984) 551;
H.-J. Möhring and J. Ranft, Nucl. Sci. Eng. 89 (1985) 247.
[33] H. Fesefeldt, Aachen Report PITHA 85/02 and Nucl. Instr. and Meth. A263 (1988) 114.
[34] G. Hartner, ZEUS-Note 88-049.